In-Flight Multi-Channel Calibration for Airborne Post-Doppler STAP

André B. C. da Silva and Stefan V. Baumgartner
Microwaves and Radar Institute, German Aerospace Center (DLR), Oberpfaffenhofen, Germany
Email: andre.silva@dlr.de

Abstract

Multi-channel calibration is essential for detecting moving targets as well as for estimating their positions and velocities accurately. This paper presents an efficient calibration algorithm for along-track multi-channel systems, in particular for space-time adaptive processing (STAP) techniques. The proposed algorithm corrects not only the phase and magnitude offsets among the receive channels, but also the Doppler centroid variation considering the range dependency and the aircraft's motion. Important parameters and offsets are estimated directly from the radar range-compressed data. The proposed algorithm is evaluated based on real multi-channel X-band data acquired by the DLR's airborne system F-SAR. The experimental results show the potential of the proposed algorithm for traffic monitoring applications.

1 Introduction

In practice, it is not possible to build absolutely identical antennas and receive channels with the same electrical characteristics and time delays. Therefore, the transfer functions and the antenna gain patterns of the receive channels differ from each other and need to be characterized or equalized [1], especially for multi-channel techniques that make use of the sum and difference channels.

For instance, the different transmitting (TX) and receiving (RX) antenna characteristics can be measured or estimated, and then incorporated into the direction-of-arrival (DOA) vector [2]. Usually, external calibration is required for compensating different time delays between the RX channels. Remaining phase and magnitude offsets can be estimated from the radar data. In addition, precise knowledge of the along-track baselines between the multiple RX channels is important for estimating DOA angles accurately, which affect the position and the velocity estimates of the targets.

Figure 1 shows the acquisition geometry of the DLR's airborne system F-SAR with four RX channels. An error on the target's DOA angle (Ψ_{DOA}) estimation may be obtained due to phase and magnitude offsets. In this case, a proper calibration algorithm is required for ensuring an accurate DOA angle estimation of the target.

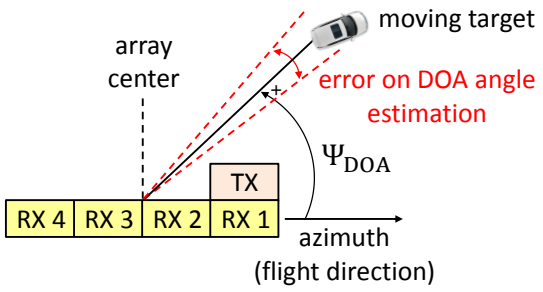

Figure 1: F-SAR acquisition geometry with four RX channels. An error on the target's DOA angle estimation may be caused by imbalances on the RX channels.

An elegant and robust method for digital channel balancing (DCB) was introduced in [3] and discussed in detail in [1]. In this method, the RX channels are balanced with respect to a reference channel by performing an iterative approach in the two-dimensional frequency domain, so that residual phase and magnitude offsets are corrected. In addition, along-track baselines among RX channels can be estimated accurately in the range-Doppler domain [1].

An interesting review about calibration techniques was presented in [4], in which simple algorithms (e.g., based on one- and two-dimensional co-registrations) and more sophisticated methodologies (e.g., DCB) were evaluated in detail for along-track interferometry (ATI), displaced phase center antenna (DPCA) and space-time adaptive processing (STAP) techniques. It is shown in [4] that the DCB achieves better performance especially in terms of clutter suppression, whereas at the expense of a much higher computational effort.

More recently, an external calibration algorithm for multi-channel airborne SAR systems was presented in [5], through which is possible to estimate accurately: the antenna baselines and attitude angles, among other parameters. The algorithm is applied on range-compressed data (i.e., no azimuth compression is required) and relies on a previously measured antenna model for proper operation. It was designed for the new DLR's airborne digital-beamforming DBF-SAR system [6].

This paper presents a fast and efficient calibration algorithm for multi-channel airborne SAR systems that is able to: 1) correct the phase and magnitude offsets among the RX channels; and 2) correct the Doppler centroid along slant range and azimuth time by using the attitude angles of the antenna array. Important parameters and offsets are estimated directly from the range-compressed data, and the estimation does not require an antenna model. Moreover, the computed offsets can be stored in the memory and be directly applied for the calibration of subsequent flights in order to speed up the processing time.

2 Calibration Algorithm

The simplified flowchart of the proposed calibration algorithm is depicted in **Figure 2**. The details about the main blocks are presented in the remainder of this section.

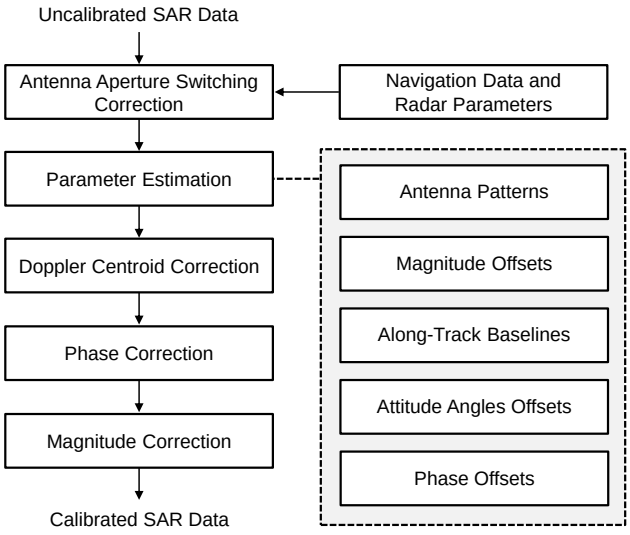

Figure 2: Main steps of the proposed calibration method.

2.1 Antenna Aperture Switching

The antenna aperture switching technique can improve the ground moving target indication (GMTI) performance of radar systems by creating additional phase centers and larger baselines. However, this operation introduces a time delay that needs to be corrected [7]. The correction can be carried out in Doppler frequency domain by applying the following phase ramp to the radar data

$$\varphi_{\mathrm{AS}}(f_{\mathrm{a}}) = \exp\{-2 \cdot \pi \cdot f_{\mathrm{a}} \cdot \Delta t_{\mathrm{AS}}\}, \qquad (1)$$

where $\Delta t_{\mathrm{AS}} = 1/(2 \cdot PRF)$ denotes the time lag introduced by the F-SAR antenna aperture switching that contributes to the effective along-track baseline and PRF is the pulse repetition frequency.

2.2 Antenna Patterns

The envelope of the two-way diagram of the azimuth antenna pattern can be estimated from the radar data by averaging all available range bins K for each Doppler frequency bin f_{a}

$$A(f_{\mathrm{a}}, m) = \sqrt{\frac{1}{K}\sum_{k=1}^{K}|\boldsymbol{z}(r_{\mathrm{k}}, f_{\mathrm{a}}, m)|^2}\ , m = 1, \dots, M, \quad (2)$$

where m denotes the index of the RX channel and $\boldsymbol{z}$ denotes the multi-channel radar data.

2.3 Magnitude Offsets

The magnitude offsets can be obtained from the azimuth antenna pattern maxima according to

$$\rho_{1,\mathrm{m}} = \frac{\max(D_{\mathrm{t}} D_{\mathrm{r},1})}{\max(D_{\mathrm{t}} D_{\mathrm{r,m}})}, m = 2, \dots, M, \qquad (3)$$

where D_{t} and $D_{\mathrm{r,m}}$ are the TX and RX antenna characteristics of the m-th channel, respectively, where the channel RX1 is assumed as reference.

The magnitude offset correction can be carried out in time domain according to

$$\boldsymbol{z}_{\mathrm{mag,corr}}(r_{\mathrm{k}}, f_{\mathrm{a}}, m) = \boldsymbol{z}(r_{\mathrm{k}}, f_{\mathrm{a}}, m) \cdot \rho_{1,m}\ , \qquad (4)$$

where $\boldsymbol{z}_{\mathrm{mag,corr}}$ denotes the radar data after magnitude correction.

2.4 Along-Track Baselines

The X-band configuration of the DLR's airborne system F-SAR has four RX channels aligned along azimuth [8].

The effective along-track baselines (i.e., $|d_{\mathrm{a1,2}}| = 0.1$ m, $|d_{\mathrm{a1,3}}| = 0.2$ m and $|d_{\mathrm{a1,4}}| = 0.3$ m) are estimated from the radar data by using the slopes of the ATI phases along Doppler frequency [1]. It is pointed out that the physical antenna center separations are twice as long.

2.5 Aircraft's Motion

The Doppler centroid variation is estimated along slant-range and along azimuth time by considering the aircraft's attitude angles: yaw, pitch and roll (cf. **Figure 3**).

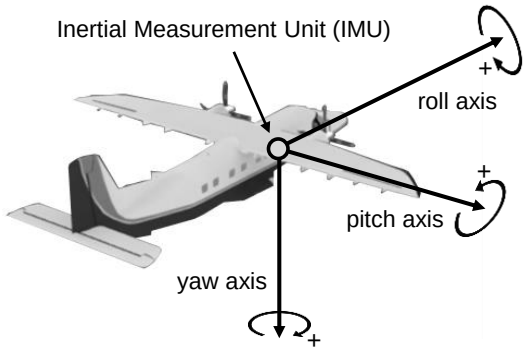

Figure 3: Aircraft's attitude angles: yaw, pitch and roll.

The F-SAR's inertial measurement unit (IMU) provides the aircraft's pitch, roll and heading angles with respect to the true North. The aircraft's heading direction can be used for obtaining the yaw angle according to

$$\theta_{\mathrm{YAW,IMU}}(t) = \theta_{\mathrm{HEADING,IMU}}(t) - \bar{\theta}_{\mathrm{COURSE}}\ , \qquad (5)$$

where $\bar{\theta}_{\mathrm{COURSE}}$ denotes the aircraft's mean flight course with respect to the true North, which is obtained according to the GPS coordinates of the aircraft.

2.6 Squint Angle and Doppler Centroid

The squint angle Ψ_{sq} and the Doppler centroid f_{DC} are generally related as

$$f_{\mathrm{DC}} = \frac{2 \cdot v_{\mathrm{p}}}{\lambda} \sin\left(\Psi_{\mathrm{sq}}\right) . \qquad (6)$$

The squint angle causes a range dependent Doppler centroid shift, which especially for large squint angles can be clearly recognized in the range-Doppler domain as a J-shaped pattern known in the literature as "J-Hook" [9].

The squint angle variation can be expressed for a left-looking antenna as

$$\Psi_{\mathrm{sq}}(r_{\mathrm{k}}, t) \approx \sin^{-1}\left[\cos\left(\theta_{\mathrm{i}}(r_{\mathrm{k}}) + \theta_{\mathrm{ROLL,ANT}}(t)\right) \tan\left(\theta_{\mathrm{PITCH,ANT}}(t)\right) + \sin\left(\theta_{\mathrm{i}}(r_{\mathrm{k}}) + \theta_{\mathrm{ROLL,ANT}}(t)\right) \cdot \tan\left(\theta_{\mathrm{YAW,ANT}}(t)\right)\right] , \qquad (7)$$

where $\theta_{\mathrm{YAW,ANT}}$, $\theta_{\mathrm{PITCH,ANT}}$ and $\theta_{\mathrm{ROLL,ANT}}$ are the yaw, pitch and roll angles of the antenna array, respectively. These attitude angles can be expressed respectively as

$$\theta_{\mathrm{YAW,ANT}}(t) = \theta_{\mathrm{YAW,IMU}}(t) + \Delta\theta_{\mathrm{YAW}} , \qquad (8)$$

$$\theta_{\mathrm{PITCH,ANT}}(t) = \theta_{\mathrm{PITCH,IMU}}(t) + \Delta\theta_{\mathrm{PITCH}} , \qquad (9)$$

$$\theta_{\mathrm{ROLL,ANT}}(t) = \theta_{\mathrm{ROLL,IMU}}(t) + \Delta\theta_{\mathrm{ROLL}} , \qquad (10)$$

where $\theta_{\mathrm{YAW,IMU}}$, $\theta_{\mathrm{PITCH,IMU}}$ and $\theta_{\mathrm{ROLL,IMU}}$ are the yaw, pitch and roll angles of the aircraft, obtained from the IMU system. Therefore, the terms $\Delta\theta_{\mathrm{YAW}}$, $\Delta\theta_{\mathrm{PITCH}}$ and $\Delta\theta_{\mathrm{ROLL}}$ are the attitude angle offsets, which need to be estimated by the proposed calibration algorithm.

In practice, the attitude angle offsets may arise due to an imperfect alignment of the antenna patches or elements, as well as due to the antenna pod's mounting on the aircraft's fuselage (i.e., non-parallel with respect to the aircraft's longitudinal axis).

The Doppler centroid variation can be expressed for a left-looking antenna as

$$f_{\mathrm{DC,ATT}}(r_{\mathrm{k}}, t) \approx \frac{2 \cdot v_{\mathrm{p}}}{\lambda}\left[\cos\left(\theta_{\mathrm{i}}(r_{\mathrm{k}}) + \theta_{\mathrm{ROLL,ANT}}(t)\right) \tan\left(\theta_{\mathrm{PITCH,ANT}}(t)\right) + \sin\left(\theta_{\mathrm{i}}(r_{\mathrm{k}}) + \theta_{\mathrm{ROLL,ANT}}(t)\right) \cdot \tan\left(\theta_{\mathrm{YAW,ANT}}(t)\right)\right] . \qquad (11)$$

Exemplarily, **Figure 4** shows a SAR image obtained in the vicinity of Memmingen, in Germany, and the Doppler centroid variation estimated according to (11). This variation needs to be corrected by the calibration algorithm.

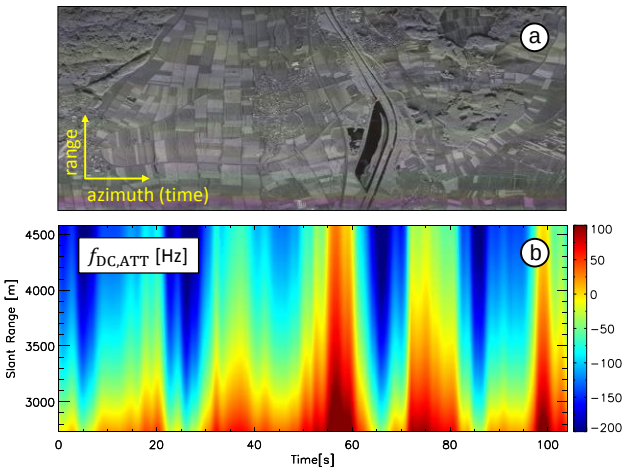

Figure 4: (a) Focused SAR image and (b) Doppler centroid estimated according to (11).

2.7 Antenna Attitude Angle Offsets

Two main steps are required for estimating the antenna attitude angle offsets ($\Delta\theta_{\mathrm{YAW}}$, $\Delta\theta_{\mathrm{PITCH}}$ and $\Delta\theta_{\mathrm{ROLL}}$):

1. A reference Doppler centroid of the scene $f_{\mathrm{DC,REF}}(r_{\mathrm{k}}, t)$ is estimated according to the reference channel RX1 (e.g., by using the energy balancing method proposed in [10]);

2. The antenna attitude angle offsets are obtained by means of multidimensional minimization (e.g., using the downhill simplex method [11])

$$\mathrm{argmin}_{\overline{\Delta\theta}}\left\{\max\left(\left\| f_{\mathrm{DC,REF}}(r_{\mathrm{k}}, t) - f_{\mathrm{DC,ATT}}(r_{\mathrm{k}}, t, \overline{\Delta\theta})\right\|\right)\right\} , \qquad (12)$$

where $f_{\mathrm{DC,REF}}(r_{\mathrm{k}}, t)$ is estimated from the radar data and $f_{\mathrm{DC,ATT}}(r_{\mathrm{k}}, t, \overline{\Delta\theta})$ is obtained from (11). The $\overline{\Delta\theta}$ dependency, denoted here explicitly, follows (8)-(10).

2.8 Phase Offsets

In practice, phase offsets can be introduced by the hardware of the radar system (e.g., connectors, cables with different lengths, thermal variation of the receiver's transfer functions, among other sources). The phase offset of each channel m with respect to RX 1 (i.e., $\varphi_{1,m,\mathrm{offset}}$) is a constant which can be estimated for the calibration flight and stored for later use. It is a property of the antenna assembly to be updated if e.g. cables are exchanged, and then assumed to be invariant between subsequent flights.

At least four main steps are necessary for estimating the phase offsets ($\varphi_{1,m,\mathrm{offset}}$) from the radar data:

1. Obtain the radar range-compressed data;
2. Select a data patch containing homogeneous clutter;
3. Compute the ATI phases for each pair of RX channels according to

$$\Delta\varphi_{1,m}(r_{\mathrm{k}}, t) = \varphi_1(r_{\mathrm{k}}, t) - \varphi_{m,\mathrm{reg}}(r_{\mathrm{k}}, t) , \qquad (13)$$

where $\varphi_{m,\mathrm{reg}}$ are the phases of the co-registered signal.

4. Estimate the phase offsets by obtaining the average value of the ATI phases

$$\varphi_{1,m,\text{offset}} = \overline{\Delta\varphi}_{1,m}(r_\text{k}, t)\ . \qquad (14)$$

2.9 Phase Correction

The phase correction (assuming the channel RX1 as reference) can be carried out in time domain according to

$$\boldsymbol{z}_{\text{ATI,corr}}(r_\text{k}, t, m) = \boldsymbol{z}(r_\text{k}, t, m) \cdot \exp\{\text{j}\Delta\hat{\varphi}_{1,m}(r_\text{k}, t)\}\ , \qquad (15)$$

where $\boldsymbol{z}_{\text{ATI,corr}}$ denotes the radar data after the phase correction and $\Delta\hat{\varphi}_{1,m}(r_\text{k}, t)$ denotes the theoretical ATI phases estimated for each pair of RX channels according to

$$\Delta\hat{\varphi}_{1,m}(r_\text{k}, t) = \frac{4\cdot\pi}{\lambda} \cdot \left[d_{\text{a1},m} \cdot \sin\left(\Psi_\text{sq}(r_\text{k}, t)\right)\right] + \varphi_{1,m,\text{offset}}\ , \qquad (16)$$

where the squint angles $\Psi_\text{sq}(r_\text{k}, t)$ are obtained according to (7) and the offsets are the constants estimated beforehand (e.g., for the calibration flight). It is important to mention that the squint angles used for the Doppler centroid correction and for the phase correction are the same.

3 Experimental Results

The proposed calibration algorithm was evaluated based on real multi-channel X-band radar data acquired with the DLR's airborne system F-SAR [8]. The flight campaign was conducted over the Memmingen's Allgäu airport, in Germany, in February 2007. A detailed experiment description and the radar parameters are found in [12].

In the post-Doppler (PD) STAP processor [13], the beamformers are applied using DOA angle steps of 0.05° within an interval determined by the azimuth antenna beam width. In the constant false alarm rate (CFAR) detector, the probability of false alarm is set to $P_\text{fa} = 10^{-6}$.

Figure 5 shows the GMTI results obtained with and without the proposed calibration algorithm, where the colors of the radar detections (circles) are related to their estimated ground range velocities. It has to be mentioned that the cars 1 to 4 moved on the edges of the airport's runway and car 5 moved off-road (in circles).

Figure 5a shows the GMTI results obtained without calibration. In this case, the phases and magnitude offsets, as well as the Doppler centroid were not corrected, resulting in systematic phase errors that extended along range and azimuth. Indeed, it is expected that the calculation and the application of the CFAR detection thresholds based on the heterogeneous clutter model presented in [14] would fail, resulting in several false detections. Furthermore, none of the cars are detected and wrong position and velocity estimates are obtained. Clearly, **Figure 5a** shows that the PD STAP performance is not acceptable without proper calibration.

Figure 5b shows much cleaner GMTI results obtained by applying the proposed calibration algorithm, where all the cars are detected several times and a few false detections are obtained. It is pointed out that most of the false detections can be discarded by using the PD STAP processor with a priori knowledge information presented in [13].

Figure 6 shows the histograms of interferometric phases obtained between channels RX1 and RX2 with and without calibration (i.e., for the scenarios shown in **Figure 5**). The histogram obtained without calibration (blue) appears shifted by a phase offset ($\varphi_{1,m,\text{offset}} = 153°$) and slightly skewed, which are typical effects of uncalibrated data [1]. The histogram obtained after applying the proposed calibration algorithm (red) is centered at zero degree (i.e., the phase offset is corrected) and presents lower variance.

To conclude, the lack of data calibration affects not only the position and the velocity estimates of the targets, but it also prevents the estimation of accurate CFAR detection thresholds, which results in an increased number of false detections. Therefore, calibration is crucial for a proper operation of the PD STAP processor.

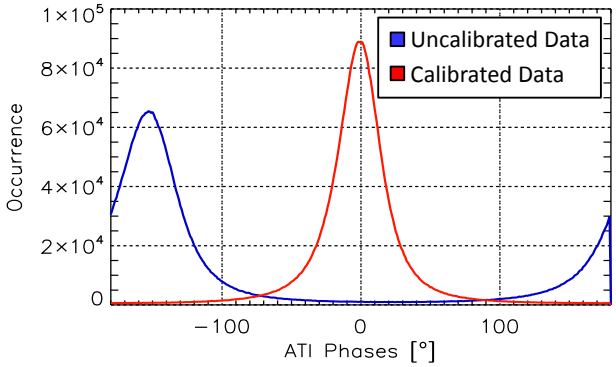

Figure 6: Histograms of interferometric phases obtained between channels RX1 and RX2 for calibrated (red) and uncalibrated data (blue) (cf. scenarios shown in **Figure 5**).

4 Conclusions

This paper presents the efficient calibration algorithm that is applied to our PD STAP processor for traffic monitoring. The proposed algorithm corrects not only the phase and magnitude offsets among the RX channels, but also the Doppler centroid by taking into account the "J-Hook" over slant range and the aircraft's motion over time. It is evaluated based on real multi-channel X-band data acquired by the DLR's airborne system F-SAR.

In the final version of this paper, the proposed calibration algorithm will be compared with the state-of-the-art DCB technique in terms of GMTI results (e.g., number of true detections and signal-to-clutter plus noise ratio - SCNR), processing time and phase correction accuracy, which is important for obtaining accurate target's phase estimation.

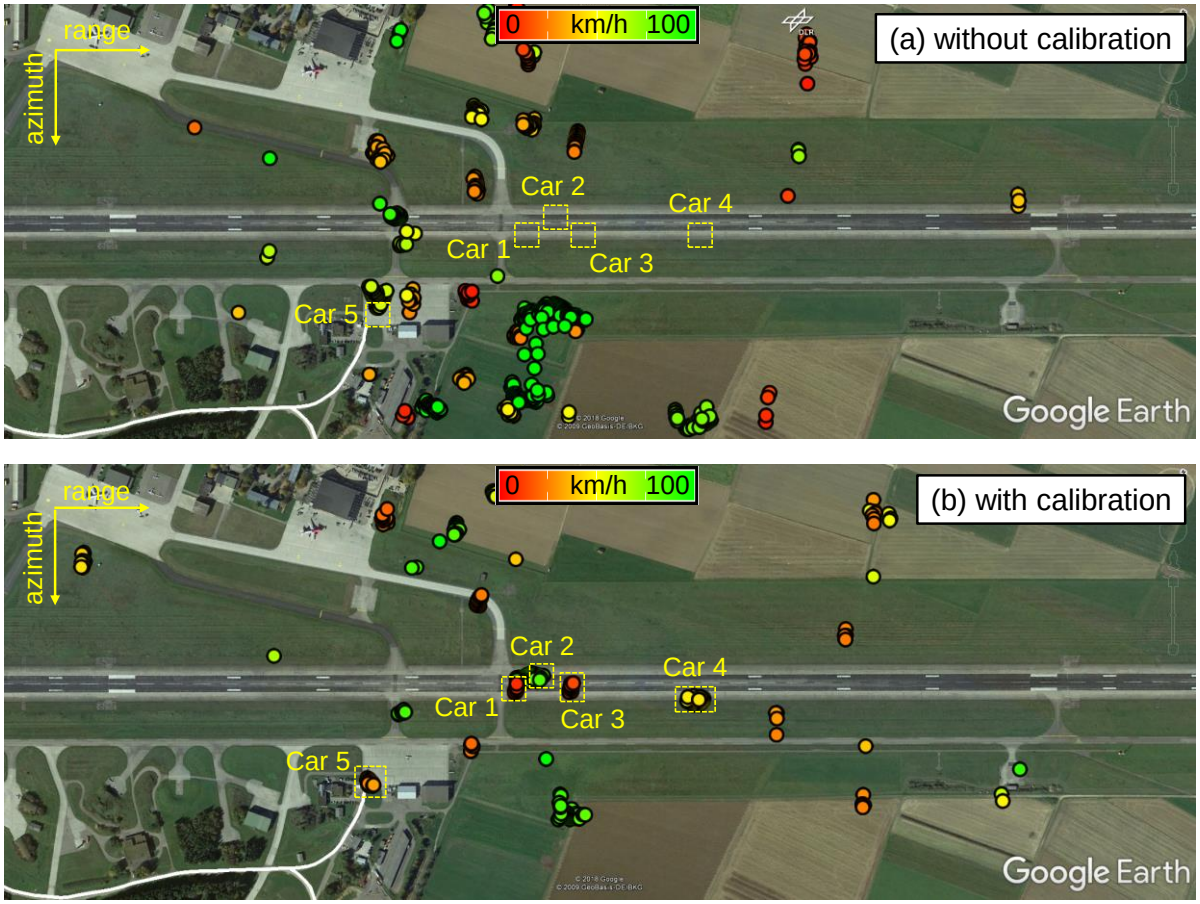

Figure 5: Google Earth images overlaid with radar detections (circles) obtained from real multi-channel X-band data: (a) without and (b) with calibration using the proposed algorithm. Clearly, the PD STAP performance is not acceptable without calibration.

References

[1] C. H. Gierull, "Digital Channel Balancing of Along-Track Interferometric SAR Data," Ottawa, Canada, 2003.

[2] J. H. G. Ender, C. H. Gierull, and D. Cerutti-Maori, "Improved space-based moving target indication via alternate transmission and receiver switching," *IEEE Trans. Geosci. Remote Sens.*, vol. 46, no. 12, pp. 3960–3974, 2008.

[3] J. H. G. Ender, "The Airborne Experimental Multi-Channel SAR-System AER-II," in *European Conference on Synthetic Aperture Radar (EUSAR)*, 1996, pp. 49–52.

[4] A. Bertetich, "Investigation of Multi-Channel SAR Calibration Methods for Real-Time Traffic Monitoring," Opera Universitaria di Trento, 2010.

[5] M. Jaeger, R. Scheiber, and A. Reigber, "External Calibration of Multi-Channel SAR Sensors Based on the Pulse-by-Pulse Analysis of Range Compressed Data Model-Based Calibration," in *European Conference on Synthetic Aperture Radar (EUSAR)*, 2018, pp. 75–78.

[6] A. Reigber *et al.*, "First Interferometric Trials with the Airborne Digital-Beamforming DBFSAR System," in *European Conference on Synthetic Aperture Radar (EUSAR)*, 2018, pp. 12–15.

[7] D. Cerutti-Maori, C. H. Gierull, and J. H. G. Ender, "Experimental verification of SAR-GMTI improvement through antenna switching," *IEEE Trans. Geosci. Remote Sens.*, vol. 48, no. 4 PART 2, pp. 2066–2075, 2010.

[8] A. Reigber *et al.*, "Very-high-resolution airborne synthetic aperture radar imaging: signal processing and applications," *Proc. IEEE*, vol. 101, no. 3, pp. 759–783, 2013.

[9] T. F. Ayoub, A. M. Haimovich, and M. L. Pugh, "Reduced-Rank STAP for High PRF Radar," *IEEE Trans. Aerosp. Electron. Syst.*, vol. 35, no. 3, pp. 953–962, 1999.

[10] R. Bamler, "Doppler Frequency Estimation and the Cramér-Rao Bound," *IEEE Trans. Geosci. Remote Sens.*, vol. 29, no. 3, pp. 385–390, 1991.

[11] J. A. Nelder and R. Mead, "A simplex method for function minimization," *Comput. J.*, vol. 7, no. 4, pp. 308–313, 1965.

[12] S. V. Baumgartner and G. Krieger, "Fast GMTI algorithm for traffic monitoring based on a priori knowledge," *IEEE Trans. Geosci. Remote Sens.*, vol. 50, no. 11, pp. 4626–4641, 2012.

[13] A. B. C. Silva and S. V. Baumgartner, "Novel post-Doppler STAP with a priori knowledge

information for traffic monitoring applications : basic idea and first results," *Adavances Radio Sci.*, vol. 15, pp. 77–82, 2017.

[14] C. H. Gierull, I. Sikaneta, and D. Cerutti-Maori, "Two-step detector for RADARSAT-2's experimental GMTI mode," *IEEE Trans. Geosci. Remote Sens.*, vol. 51, no. 1, pp. 436–454, 2013.